BRAIN CONNECTIVITY
Volume 12, Number 10, 2022
Mary Ann Liebert, Inc.
DOI: 10.1089/brain.2021.0125

ORIGINAL ARTICLES

Open camera or QR reader and scan code to access this article and other resources online.

Variability in Resting-State Functional Magnetic Resonance Imaging: The Effect of Body Mass, Blood Pressure, Hematocrit, and Glycated Hemoglobin on Hemodynamic and Neuronal Parameters

Guro Stensby Sjuls[1–3] and Karsten Specht[1,2,4]

Abstract

Introduction: Replicability has become an increasing focus within the scientific communities with the ongoing ''replication crisis.'' One area that appears to struggle with unreliable results is resting-state functional magnetic resonance imaging (rs-fMRI). Therefore, the current study aimed at improving the knowledge of endogenous factors that contribute to inter-individual variability.
Methods: Arterial blood pressure (BP), body mass, hematocrit, and glycated hemoglobin were investigated as potential sources of between-subject variability in rs-fMRI, in healthy individuals. Whether changes in resting-state networks (rs-networks) could be attributed to variability in the blood-oxygen-level-dependent (BOLD)-signal, changes in neuronal activity, or both was of special interest. Within-subject parameters were estimated by utilizing dynamic-causal modeling, as it allows to make inferences on the estimated hemodynamic (BOLD-signal dynamics) and neuronal parameters (effective connectivity) separately.
Results: The results of the analyses imply that BP and body mass can cause between-subject and between-group variability in the BOLD-signal and that all the included factors can affect the underlying connectivity.
Discussion: Given the results of the current and previous studies, rs-fMRI results appear to be susceptible to a range of factors, which is likely to contribute to the low degree of replicability of these studies. Interestingly, the highest degree of variability seems to appear within the much-studied default mode network and its connections to other networks.

Keywords: blood pressure; BMI; dynamic-causal modelling; glycated hemoglobin; hematocrit; resting-state functional magnetic resonance imaging; resting-state network; resting-state variability

Impact Statement

We believe that thanks to the evidence that we have collected by analyzing the well-controlled data of the Human Connectome Project with dynamic-causal modeling (DCM) and by focusing not only on the effective connectivity, which is the

[1]Department of Biological and Medical Psychology, University of Bergen, Bergen, Norway.
[2]Mohn Medical and Imaging Visualization Centre, Haukeland University Hospital, Bergen, Norway.
[3]Language Acquisition and Language Processing Lab, Department of Language and Literature, Norwegian University of Science and Technology, Trondheim, Norway.
[4]Department of Education, UiT/The Arctic University of Norway, Tromsø, Norway.
A preprint of this article was uploaded to the preprint server *bioRxiv* (https://www.biorxiv.org/content/10.1101/2021.06.02.446721v1).

typical way of using DCM, but also by analyzing the underlying hemodynamic parameters, we were able to explore the underlying vascular dependencies in a much broader perspective. Our results challenge the premise for studying changes in the default mode network as a clinical marker of disease, and we add to the growing list of factors that contribute to resting-state network variability.

Introduction

When studying the resting brain by utilizing resting-state functional magnetic resonance imaging (rs-fMRI), the brain's energy consumption is measured as the participant is resting in an MR-scanner (Biswal et al., 1995). This activity fluctuates in a range below 0.1 Hz, and it is hypothesized to support communication among neurons in the absence of a specific task (Biswal et al., 1995; Raichle and Mintun, 2006). The measured time-series of the fluctuations can further be analyzed and organized into fairly consistent resting-state networks (rs-networks) (Allen et al., 2011).

Resting-state networks

The growth of rs-fMRI studies over the past decades can, in part, be explained by the discovery of a consistent, functionally connected pattern of distributed brain regions as a persistent network of ''deactivation.'' The activation of this default mode network (DMN) ceases when a goal-directed or attention-demanding behavior or task is initiated (Raichle et al., 2001). Although there is no unified view of the function of the DMN as of yet, it has been postulated to support a ''default mode'' of the brain when an individual is awake and alert, but not actively involved in a task (Raichle et al., 2001).

Others have suggested the DMN to be involved in a self-referential and introspective state (Greicius et al., 2003; Singh and Fawcett, 2008), involved in mediating the processes where one, for example, retrieves memories, plans for the future, or processing of one's own impressions and feelings (Buckner et al., 2008).

As the DMN is ''deactivated'' when a cognitive task is performed, the activation of the central executive network (CEN) is increasing, and the anti-correlation between the DMN and the CEN has been shown to increase with the degree of task difficulty (Fox et al., 2005). The CEN is a task-related network, and it is believed to be involved in the manipulation and maintenance of information in working memory (Bressler and Menon, 2010; Toro et al., 2008). It is further postulated to be involved in decision making in goal-directed behavior, attention, response inhibition, and other executive functions, which qualitatively separates it from the DMN (Bressler and Menon, 2010; Koechlin and Summerfield, 2007).

The salience network (SN) is involved in the bottom-up detection of salience, by directing attention and memory resources to salient events. It has been shown to play a mediating role in the up- and downregulation of the DMN and the CEN (Sridharan et al., 2008), as a possible link between stimulus-driven processing and monitoring the internal environment of the brain and body (Craig, 2009; Menon and Uddin, 2010).

Endogenous sources of variability in rs-fMRI

Despite its recent rise in popularity, the results of rs-fMRI seem to show between- and within-subject variability with a variety of endogenous and exogenous factors (Specht, 2019). Given that the blood-oxygen-level-dependent (BOLD)-signal measured with fMRI is merely related to neuronal activity, and actually arises from a combination of changes in cerebral blood flow (CBF), cerebral blood volume (CBV), and oxidative metabolism to meet the energy demands of the active brain (Gauthier and Fan, 2019), other factors that can contribute to changes in CBF and CBV, for example, arterial blood pressure (BP), body mass and fat, and the velocity of the blood, might impact the BOLD-signal, and in turn the rs-fMRI results (Buxton et al., 1998).

Several mathematical models of the hemodynamic response have been proposed to better understand and make predictions about the intricate relationship between neuronal and hemodynamic responses. Among these are the non-linear Balloon model (Buxton et al., 1998), which treats the venous compartments as a balloon that inflates due to increased CBF. The CBV therefore increases, and as a consequence deoxygenated hemoglobin (dHb) is released at a faster rate. In turn, this affects the BOLD-signal, essentially prolonging it (Buxton et al., 2004). Factors that can affect CBV and CBF, such as body mass index (BMI) and BP, are put forward in the model as affecting the BOLD-signal (Buxton, 2012).

In addition to possibly affecting the BOLD-signal dynamics, some studies also imply that the connectivity between and within rs-networks can change with several endogenous factors. The relationship between BP and connectivity in the rs-networks, in normotensive individuals, has, to the best of the authors' knowledge, not been investigated. However, several studies have been conducted on individuals with hypertension, employing both rs-fMRI, rat models and functional near-infrared spectroscopy (Bu et al., 2018; Carnevale et al., 2020; Huang et al., 2016).

Hematocrit (HCT) levels have been associated with regional differences in functional connectivity. Regions associated with the DMN, the CEN and the SN, namely the anterior cingulate cortex (ACC), and the medial prefrontal cortex (mPFC), the intraparietal sulcus, the insula, and the opercular cortex, have been found to show between-subject variation with HCT levels (Yang et al., 2015). Yang and colleagues (2015) rightly point out that it is unclear whether these differences are due to neuronal or non-neuronal variation.

Some studies have found higher BMI to be related to decreased within-network connectivity of the DMN, the CEN and the SN, as well as increased between-network connectivity (Chao et al., 2018; Doucet et al., 2017; Sadler et al., 2018). However, the regions included in these studies, as well as the results, vary. Still, several of the authors hypothesize that higher BMI is linked to changes in networks that balance sensory-driven and internally guided states (the CEN and the DMN, respectively), a role often attributed to the SN. This might lead to weight gain as a consequence of poorly regulated eating behavior (Doucet et al., 2017; Sadler et al., 2018).

Glycated hemoglobin (HbA1c) and changes in rs-fMRI connectivity have been studied by comparing pre-diabetic or diabetic individuals (HbA1c 5.7–6.4) with healthy individuals (Sadler et al., 2019). Similar to the conclusions drawn from the previously mentioned BMI results, the authors discuss whether differences between groups are associated with differences in self-control; the functional connectivity pattern of the healthy individuals shows stronger functional connectivity between a ventral attention network and a cingulo-opercular network (including regions of the SN [insula] and the CEN [DLPFC]), whereas the functional connectivity pattern of prediabetic individuals has been found to be stronger between the ventral attention network, a visual and a somatosensory network.

However, as compared with the results for BMI, no difference in DMN activity was observed (Sadler et al., 2019). Individuals with type 2 diabetes mellitus have also been found to exhibit weaker functional connectivity in the right insula (region within the SN), and from the right insula to the bilateral superior parietal lobule, compared with healthy individuals (Liu et al., 2017).

The replication crisis in the field of rs-fMRI

As BP, HCT, BMI, and HbA1c possibly affect cerebral hemodynamics, which could affect and disturb the BOLD-signal, it is uncertain whether the previous results on functional connectivity really represent changes in neuronal activity. If the results can be ascribed to changes in cerebral hemodynamics, the results mentioned earlier might have been wrongly attributed to changes in neuronal activity. In effect, rs-variability relates to the ongoing replication crisis in the field of psychological and medical research.

Several studies indicate that rs-fMRI studies seem to produce highly unreliable results, showing within- and between-subject variability with a range of different endogenous and exogenous factors. These include the time of year and the time of day, circadian rhythm, sleep duration, prior events, mood, age, and gender, to mention only a few (Agcaoglu et al., 2015; Choe et al., 2015; Curtis et al., 2016; Goldstone et al., 2016; Harrison et al., 2008; Hodkinson et al., 2014; Waites et al., 2005). Arguably, these findings give rise to skepticism about the rs-networks presumed stability (Specht, 2019).

Toward higher replicability within the field of rs-fMRI

To further increase the knowledge on between-subject variability in the rs-networks of healthy individuals, the effects of BP, HCT, BMI, and HbA1c were investigated in this study. A research procedure that allows for functionally separating the BOLD-signal variation that can be attributed to hemodynamics, and the BOLD-signal variation that can be attributed to neuronal activity, was considered as highly relevant: First, if some of the variation ascribed to variance in functional connectivity might, in fact, be attributable to hemodynamic variance, the conclusions drawn from functional connectivity studies might be flawed.

Second, if the variables cause variability in both the hemodynamic and neuronal parameters of the BOLD-signal, it would imply that at least some of the variation in the hemodynamic parameters should be accounted for when drawing conclusions on connectivity. Third, if all of the potentially observed variability can be ascribed to the neuronal parameters of the BOLD-signal, it could potentially confirm previous studies on rs-connectivity. And finally, a study that aims at ascribing the potential variability caused by some endogenous factors to either the hemodynamic response independently of neuronal activity, or the neuronal activity in rs-networks, has not previously been conducted.

The current study aimed at investigating the between-subject variability that BP, HCT, BMI, and HbA1c might cause in large scale rs-networks, as well as the between-group variability potentially caused by BMI, in a healthy population. The overarching implications of the current study relate to the ongoing replication crisis and what measures can be taken to ensure more reliable results in the fast-growing field of rs-fMRI, essentially facilitating more reliable results for future studies.

Hypotheses

Increased BP, BMI, HbA1c, and HCT can affect the rate at which oxygenated hemoglobin (oHb) is being utilized in the capillaries and dHb is transported to the veins, affecting the response from the venous compartments, given the Balloon model of the BOLD-signal (Buxton et al., 1998). It was hypothesized that increased BP, BMI, and HbA1c will weaken the BOLD-signal (H_1, H_2, H_3, respectively), as higher BP can represent increased segmental vascular resistance, and increased BMI can decrease the CBV, as a non-linear negative correlation has been found for body weight and blood volume (Lemmens et al., 2006).

As BMI affects CBV, it is included in the Balloon model, as a factor that might affect the BOLD-signal (Buxton et al., 1998). Given the assumed correlation between BMI (and body fat) and HbA1c (Iso et al., 1991; Lalande et al., 2010), we predict the same relationship for HbA1c, namely weakened BOLD-signal with increased HbA1c scores. Increased HCT scores, on the other hand, was hypothesized to strengthen the BOLD-signal (H_4). HCT is an indicator of the amount of Hb available and the blood's capacity to transport O_2.

When HCT is low, the blood will lose some of its ability to transport O_2; however, when HCT is high, the blood is able to transport more O_2 (González-Alonso et al., 2006). Studies on the relationship between baseline HCT and the BOLD-signal have found it to be contributing to the degree of BOLD-activation (Levin et al., 2001; Xu et al., 2018; Zhao et al., 2007). These studies implicate a positive relationship between the BOLD-signal activation and HCT levels, specifically in men, in task-based fMRI.

Further, some hypotheses for the neuronal parameters were postulated based on the literature described in the ''Endogenous Sources of Variability in rs-fMRI''-section. As we are not aware of any studies on the relationship between BP and rs-network connectivity, no hypothesis was made for this relationship. For HCT, it was hypothesized that increased HCT values would weaken the internal connectivity of the DMN, the CEN and the SN (H_5). As no study, to the best of our knowledge, has investigated the relationship between HCT values and between-network connectivity, specific prediction was not made for this relationship.

Previous results with regards to changes in connectivity associated with BMI are, as mentioned, varied, in terms of both included networks and their results. However, the

most often found, and therefore the presumably most robust, result from the literature indicates that increased BMI is associated with a weakening of the SN; the network is associated with balancing sensory-driven and internally guided states (the CEN and the DMN, respectively).

This result is often accompanied with a weakening of the internal connectivity of DMN and a strengthening of the connectivity between these two networks. It is, therefore, hypothesized that increased BMI will weaken the internal connectivity of the DMN and the SN, while strengthening the between-network connectivity (H_6).

For HbA1c, no alterations in the DMN have been observed with increased (prediabetic/diabetic) HbA1c values. However, a weakening of the SN and the CEN has been indicated by previous studies. In healthy individuals, a strengthening of between-network connections for regions within the SN and the CEN has been found, which was not observed in prediabetic individuals. It is therefore, finally, hypothesized that increased HbA1c values will weaken the internal connectivity of the SN and the CEN, and weaken the between-network connectivity (H_7). However, the relationship might not be as evident from the current study, as only healthy individuals' HbA1c scores will be compared.

To investigate these hypotheses, a hierarchical between-subject and between-group (based on BMI) design was chosen, based on the parameters from a cross-spectral density dynamic-causal modeling (csd-DCM) analysis. Generally speaking, DCM is a generative model that infers on hidden neuronal states and activity given the measured fMRI signal (Friston, 2009). For rs-fMRI, this framework has recently been extended to infer on effective connectivity, by parametrizing the spectral characteristics of the neuronal fluctuations (Friston et al., 2014; Razi et al., 2015).

Such a csd-DCM is superior to other methods in this context, since it allows to separately examine the individual parameters of the hemodynamic response, effective connectivity, csd parameters α (amplitude) and β (density of the neural fluctuations), and free energy (model evidence), and their relationship to the endogenous factors BP, HCT, BMI, and HbA1.

Methods

A large sample of healthy young subjects were studied, to give indications of variability within a normal population, and to ensure the study's statistical power. After ethical and practical considerations, previously collected data from the Human Connectome Project (HCP) were considered sufficient to answer the research question. Information on the subjects and the data collection protocols are available online, allowing transparency and insight into the potential advantages and disadvantages of the data used (Van Essen et al., 2013).

Subjects

The data used in the current study stem from the HCP S1200 release, which consists of data from healthy subjects from families with twins, born in the Missouri area (U.S.) and ranging from 22 to 35 years of age (Van Essen et al., 2013). A subsample ($N = 594$) was semi-randomly chosen on the basis of an equal distribution of gender and age, as a part of a study on time-of-day effects on rs-fMRI effective connectivity and hemodynamic response.

Therefore, the participants were also equally distributed throughout the day, in terms of scanning times (from 09.00 to 21.00) (for details, see Vaisvilaite et al., 2021). Individuals with diabetes and high BP were excluded from the HCP data collection ''as these might negatively impact neuroimaging data quality.'' However, subjects with undiagnosed high BP and diabetes kept under control by means of diet were included in the study.

The study sample ($N = 594$) was similar to the total HCP sample ($N = 1206$) in terms of BP, HCT, BMI, and HbA1c, in addition to having a similar distribution of gender and age: full sample ($N = 1206$; female = 656, male = 550, mean age = 28.8; SD = 3.6), study sample ($N = 594$, female = 310, male = 284, mean age = 28.8; SD = 3.6). For more information on recruitment, inclusion and exclusion criteria, protocols for the data collection, and image acquisition for the MR-scans, please see Uğurbil and colleagues (2013) and Van Essen and colleagues (2012, 2013). This study was approved by the regional ethics committee for medical research.

Image processing

The current study utilized the minimally pre-processed HCP data (HCP Minimal Pre-processing Pipeline); for more information please see Glasser and colleagues (2013). All further processing was performed within SPM12 in MATLAB and included smoothing with a 6 mm full width at half maximum Gaussian kernel and denoising, before extracting the time-series for the DCM analysis. For denoising the data, a two-step general linear model (GLM) was specified to regress out non-gray matter sources of noise and movement artefacts.

Two regions of interest (ROIs, sphere with a radius of 6 mm) were specified for each subject, one within the white matter (Montreal Neurological Institute [MNI] coordinates: $[0 - 24 - 33]$) and one within the cerebrospinal fluid (MNI coordinate: $[0 - 40 - 5]$). To control for subject movement in the course of the scanning session, the 12 movement parameters, which are provided with the dataset and which are based on the initial realignment of the raw data, were included in the GLM analysis. As the rs-data were acquired in two scanning sessions per individual (Van Essen et al., 2012), the preprocessing steps were performed separately for each of the sessions (Left/Right and Right/Left phase encoding) and for each individual separately.

DCM analyses

To study the effects of BP, HCT, BMI, and HbA1c on the hemodynamics and effective connectivity in three large-scale rs-networks, the rs-fMRI time-series from eight ROIs (sphere with a radius of 6 mm) were extracted. See Table 1 for the coordinates for each region and which network they are a part of. These networks and their coordinates were chosen based on their assumed importance in several clinical conditions (Menon, 2011). The number of included ROIs was limited to eight due to computational strain.

The time-series of each ROI were extracted and subjected to individual csd-DCM analyses, and the csd-DCMs were specified for each rs-fMRI acquisition separately. Each subject underwent two rs-fMRI acquisitions, and a total of 1188

Table 1. Coordinates for Regions of Interest

Resting-state network	*Regions*	*R/L*	*MNI coordinates* (x, y, z)
Default mode network	PCC	R/L	0, −52, 26
	mPFC	R/L	3, 54, −2
	LIPC	L	−50, −63, 32
	RIPC	R	48, −69, 35
Central executive network	DLPFC	R	45, 16, 45
	PPC	R	54, −50, 50
Salience network	AI	R	37, 25, −4
	ACC	R/L	4, 30, 30

The coordinates for each ROI, and which rs-network the given regions are considered a part of.

ACC, anterior cingulate cortex; AI, anterior insular cortex; DLPFC, dorsolateral prefrontal cortex; L, left hemisphere; LIPC, left inferior parietal cortex; MNI, Montreal Neurological Institute; mPFC, medial prefrontal cortex; PCC, posterior cingulate cortex; PPC, posterior parietal cortex; R, right hemisphere; RIPC, right inferior parietal cortex; ROI, region of interest.

acquisitions were included in the analysis. This was done to improve the robustness of the DCM estimation by exploring only the averaged effects across the two acquisitions. Please note, both acquisitions were done within the same session (session 1). In the current study, the *priors* were turned on for connections between all the included regions.

The csd-DCM resulted in parameters of effective connectivity between and within each region (A-matrix) and hemodynamic parameters (transit time for each region, epsilon, and decay). In addition, csd-values (α- and β-values) and Free Energy parameters were extracted.

The effective connectivity (A-matrix) refers to the correlation in the frequency distribution of the BOLD-signal between brain regions. As the activity in one region is being modeled as a function of the frequency distribution in another region, it indicates the causal interference that one brain region makes on another (Friston et al., 2014; Zeidman et al., 2019a). The hemodynamic parameters are essentially descriptions of the Balloon Model, which is incorporated in the DCM framework and which is essential for the DCM parameter estimation.

The hemodynamic response, as estimated by the DCM and stated in the hemodynamic state equation (Stephan et al., 2007), can be identified as: the transit time for each predefined region (resting CBV divided by resting CBF, as a measure of BOLD-signal dynamics), decay as the global parameter of the BOLD-signal (the reduction of the BOLD-signal, which relates to the relaxation of the smooth musculature of the arterioles), and epsilon as the neuronal efficacy (the relationship between CBF and neuronal activity, reflecting an increase in relative CBF expressed as a number of transients per second) (Friston et al., 2000; Zeidman et al., 2019a).

The spectral density values, expressed as α- and β-values, reflect the amplitudes and exponents of the spectral density of the neuronal fluctuations, respectively. Further, model evidence, expressed as ''Free Energy,'' is calculated (Friston et al., 2014). For DCM analyses, the Free Energy appears to be a better estimate for model evidence than alternative approaches such as Akaike's Information Criterion or the Bayesian Information Criterion (Penny, 2012).

Statistical analyses

To test the hypotheses of between-subject variation in the DCM parameters, a hierarchical linear regression analysis was conducted. As some relationship between the independent and dependent variables is assumed, a hierarchical linear regression analysis was only conducted on the independent variables (BP, HCT, BMI, and HbA1c) and the dependent variables (DCM parameters) that showed a significant correlation (Pearson two-tailed $p < 0.05$). The effective connectivity parameters left inferior parietal cortex (LIPC) to ACC, right inferior parietal cortex (RIPC), and PPC to mPFC did not meet the assumptions of linear regression and were, therefore, not included in the final regression analysis.

If more than one independent variable correlated significantly with the same dependent variable, both were added to the same regression model, while controlling for the effect of gender. For the full models (including the independent variable(s) and gender), it was examined as to which of the variables made a significant unique contribution to explaining the variance in the dependent variable, and whether the full model significantly predicted the dependent variable. To investigate the relative contribution of each factor independently, the standardized beta coefficients were examined for each model.

The value quantifies the unique contribution that each independent variable makes to the full model, and the related sig.-value allows for determining whether the contribution was significant. The R^2 change for full models was examined to determine whether the independent variables made a significant contribution to the model, after controlling for gender. Extreme outliers, defined as >3.0 interquartile from the mean, were removed. The unadjusted α-value was set to 0.05, and the confidence interval was set to 95%. Multiple testing was not controlled for; however, the results significant at the stricter 0.01 α-value are marked with double asterisks in Table 2.

In addition, a Kruskal–Wallis H test of between-group variance was conducted, comparing three BMI groups on the DCM parameters. A non-parametric test was chosen over a parametric test of group comparison, as the groups were not normally distributed. The BMI variable was split into three groups: normal weight (BMI 19–24, $n = 262$), overweight (BMI 25–29, $n = 202$), and obese (BMI >30, $n = 117$), for comparison. The χ^2-distribution was defined by the *degrees of freedom* (K − 1), which in this case was 2.

In the cases of significant group differences, a pairwise comparison with Bonferroni corrections was used to investigate which groups significantly differed ($p < 0.05$). The Mean Rank Value was used to determine which of the groups showed a higher rank order, and effect sizes were calculated ($r = z/\sqrt{n + n}$) (see Supplementary Fig. S1 for the frequency distribution of the groups across BMI scores/groups).

Results

Descriptive statistics

A two-tailed Pearson correlation analysis was conducted with the independent variables (confidence interval = 95%). It revealed a significant relationship ($p < 0.05$) between systolic BP and HCT ($r = 0.105$, $p = 0.015$) and between systolic BP and BMI ($r = 0.335$, $p = 0.000$). There was also a significant relationship between diastolic BP and HCT ($r = 0.085$, $p = 0.048$) and between diastolic BP and BMI ($r = 0.291$,

Table 2. Regression Table for Significant Results

		Modell summary					*Coefficients*	
	Model	R^2	R^2 *change*	(df *reg,* df *res)* = F	*Sig.*	*Sig.* F *change*	β	*Sig.*
A. Hemodynamic parameters								
PCC transit time	Gender	0.010	0.009	(2, 578) = 2.936	0.054	0.021*	0.035	0.396
	BMI[a]						−0.096	0.021*
mPFC transit time	Gender	0.028	0.028	(3, 573) = 5.567	0.001**	0.000**	0.028	0.497
	Dia BP						−0.130	0.003**
	BMI						0.157	0.000**
LIPC transit time	Gender	0.006	0.006	(2, 575) = 1.803	0.166	0.060	0.002	0.961
	Dia BP						−0.079	0.060
RIPC transit time	Gender	0.013	0.005	(2, 575) = 3.707	0.025*	0.034*	−0.065	0.133
	Sys BP						−0.074	0.090
AI transit time	Gender	0.013	0.013	(2, 575) = 2.936	0.020*	0.006**	0.036	0.391
	Dia BP						−0.116	0.006**
DLPFC transit time	Gender	0.006	0.005	(2, 575) = 2.679	0.069	0.085	0.053	0.211
	Dia BP						0.073	0.085
PPC transit time	Gender	0.010	0.006	(2, 575) = 3.013	0.050	0.059	0.052	0.213
	Dia BP[b]						0.080	0.059
Decay	Gender	0.009	0.008	(2, 575) = 2.683	0.069	0.028*	−0.045	0.286
	Dia BP						0.092	0.028*
Epsilon	Gender	0.017	0.017	(2, 575) = 3.400	0.018*	0.007**	−0.014	0.749
	Dia BP						0.123	0.034*
	Sys BP						0.015	0.804
B. Effective connectivity parameters								
PCC to PPC	Gender	0.016	0.010	(2, 409) = 3.393	0.035*	0.047*	−0.077	119
	HbA1c						0.098	0.047*
mPFC	Gender	0.017	0.016	(2, 572) = 4.989	0.007**	0.002**	−0.045	0.285
	Dia BP						0.130	0.002**
mPFC to PCC	Gender	0.011	0.011	(2, 578) = 3.150	0.044*	0.013*	−0.014	0.739
	BMI						0.104	0.013*
LIPC to RIPC	Gender	0.013	0.012	(2, 533) = 3.514	0.030*	0.013*	0.031	547
	HCT						−0.128	0.013*
ACC to RIPC	Gender	0.013	0.012	(2, 575) = 3.745	0.024*	0.009**	−0.001	0.974
	Sys BP						0.114	0.009**
RIPC to mPFC	Gender	0.019	0.011	(2, 575) = 5.648	0.004**	0.004**	−0.057	0.188
	Sys BP						−0.110	0.011*
C. Cross-spectral density values								
Alpha (α)	Gender	0.013	0.011	(2, 575) = 3.759	0.024*	0.012*	−0.062	0.139
	Dia BP						0.105	0.012*
Beta (β)	Gender	0.013	0.011	(3, 573) = 2.498	0.059	0.044*	−0.062	0.139
	Dia BP[c]						0.105	0.019*
	BMI						0.002	0.963
D. Free energy								
Free energy	Gender	0.079	0.050	(6, 400) = 5.750	0.001**	0.001**	−0.162	0.007**
	Dia BP						0.104	0.124
	Sys BP						0.053	0.457
	BMI						0.096	0.068
	HCT						−0.081	0.157
	HbA1c						0.060	0.217

Results from the regression analysis. See Supplementary Table S3A for the contribution of gender as predictor alone for these and notice the R^2. Change values in the current table for the change in explained variance by the full model as compared with gender alone. See Supplementary Table S3B–D for all the regressions with effective connectivity parameters, including the cases where gender significantly predicted effective connectivity parameters alone. Confidence interval = 95%.

A. Results for the hemodynamic parameter transit time for each of the included regions, and decay and epsilon.

B. Results for the effective connectivity parameters where the full models contributed significantly to predicting the outcome variable, with the independent variables making a unique significant contribution to explaining the variance.

C. The results for the cross-spectral density values. Diastolic BP made a significant unique contribution to the model, and the full model was close to statistically significant.

D. The results for the free energy parameter.

[a]BMI made a uniquely significant contribution to the model. The full model was not statistically significant, but it indicated a strong trend.

[b]Adding diastolic BP to the model did not explain significantly more of the variance in PPC transit time than gender alone, but it was close to statistically significant. The full model was also very close to statistically significant.

[c]Diastolic BP made a significant unique contribution to the model, and the full model was close to statistically significant.

*$p < 0.05$, **$p < 0.01$.

AI, anterior insula; β, standardized coefficient beta; BMI, body mass index; *df* reg, degrees of freedom regression; *df* res, degrees of freedom residual; Dia BP, diastolic blood pressure; HbA1c, glycated hemoglobin; HCT, hematocrit; PCC, posterior cingulate cortex; PPC, posterior parietal cortex.; Sys BP, systolic blood pressure.

$p = 0.000$). Systolic and diastolic BP had the strongest significant covariation ($r = 0.680$, $p = 0.000$) (see Supplementary Table S1 for the full correlation matrix).

Hemodynamic parameters

For mPFC transit time, adding BMI and diastolic BP explained significantly more of the variance. Both variables made significant unique contributions to the model, and the full model was significant; diastolic BP and BMI together explained 2.8% of the variance. For AI transit time, adding diastolic BP to the model made a significant, unique, contribution to explaining the variance, and the full model was significant, explaining 1.3% of the variance.

For the remaining hemodynamic parameters, namely decay and epsilon, diastolic BP and systolic BP made a significant contribution to the model for epsilon, with diastolic BP making a significant unique contribution to explaining the variance. The full model was significant, explaining 1.7% of the variance. See Table 2A for the regression table for these parameters.

The only hemodynamic parameter that differed between BMI groups was PCC transit time (normal weight $n = 262$, overweight $n = 202$, obese $n = 117$), χ^2 ($df = 2$, $n = 581$) $= 8.718$, $p = 0.013$. After the pairwise comparison with Bonferroni correction, the significant difference between the groups was found between the overweight and the obese groups, with the overweight group having a higher mean rank value (mean rank = 314) than the obese group (mean rank = 258), $p = 0.009$, $r = 0.166$ (see Supplementary Table S2 for the Kruskal–Wallis H tests with all hemodynamic parameters).

Effective connectivity parameters

The regressions with effective connectivity parameters as outcome variables revealed some of the independent variables to contribute significantly to explaining more of the variance in the given parameter than gender, and that one or more of the independent variables contributed significantly to this tendency, with the full model (including gender) being significant ($p = >0.05$). HbA1c made a significant contribution to explaining the variance in PCC to PPC effective connectivity, explaining 1.0% of the variance.

Diastolic BP significantly contributed toward explaining the variance in mPFC, explaining 1.6% of the variance. BMI made a significant contribution to explaining the variance in mPFC to PCC, explaining 1.1% of the variance. HCT made a significant contribution to explaining the variance in LIPC to RIPC, explaining 1.2% of the variance. Systolic BP made a significant contribution to explaining the variance in ACC to RIPC, explaining 1.2% of the variance. Systolic BP made a

Table 3. Sig. Kruskal–Wallis H Tests with Effective Connectivity Parameters, with sig. Group Differences

	Kruskal–Wallis			*Pairwise comparisons*			
Connections	*Sig.*	χ^2	*Pairwise comparison*	*Std. Stat.*	*Adj. Sig*	*r*	*Mean rank*
PCC to mPFC	0.011*	8.938	NW–OB	1.598	0.330	0.166	NW: 289.84
			OW–OB	2.966	0.009**		OW: 316.00
			NW–OW	−1.648	0.298		OB: 260.39
PCC to RIPC	0.003**	11.594	NW–OB	2.164	0.091	0.190	NW: 292.99
			OW–OB	3.405	0.002**		OW: 316.92
			NW–OW	−1.509	0.394		OB: 253.09
RIPC	0.002**	12.476	NW–OB	1.067	0.857	0.183	NW: 281.88
			OW–OB	3.277	0.003**	−0.122	OW: 323.64
			NW–OW	−2.632	0.025*		OB: 262.21
PCC to DLPFC	0.030*	7.042	NW–OB	2.566	0.031*	0.131	NW: 306.07
			OW–OB	2.155	0.094		OW: 299.17
			NW–OW	0.435	1.000		OB: 258.78
mPFC to RIPC	0.032*	6.899	NW–OB	−2.610	0.027*	0.134	NW: 274.42
			OW–OB	−1.431	0.457		OW: 295.70
			NW–OW	−1.341	0.539		OB: 322.52
LIPC to PCC	0.013*	8.637	NW–OB	1.601	0.328	0.134	NW: 316.65
			OW–OB	−0883	1.000		OW: 270.58
			NW–OW	2.904	0.004**		OB: 287.13
LIPC to mPFC	0.010**	9.290	NW–OB	0.769	1.000	0.139	NW: 313.84
			OW–OB	−1.787	0.222		OW: 266.16
			NW–OW	3.005	0.008**		OB: 299.65
LIPC	0.040*	6.435	—	—	—	—	—
LIPC to RIPC	0.041*	6.409	NW–OB	1.556	0.359	0.114	NW: 313.85
			OW–OB	−0551	1.000		OW: 274.83
			NW–OW	2.460	0.042*		OB: 285.16
AI to mPFC	0.009**	9.368	NW–OB	−1.596	0.331	−0.140	NW: 268.59
			OW–OB	1.000	0.952		OW: 316.76
			NW–OW	−3.037	0.007**		OB: 298.02

The significant Kruskal–Wallis H test for BMI group differences in the effective connectivity parameters, and the pairwise comparison statistics. Total $N = 585$, NW $n = 262$, OW $n = 202$, OB $n = 117$. Degrees of freedom = 2. Std. Stat. = standardized test statistic. Adj.Sig = adjusted α-value after Bonferroni Correction. r = effect size. Dash indicates no data obtained, as the pairwise comparison was not run. Please see Supplementary Table S4 for the non-significant results. *$p = 0.05$, **$p = 0.01$.

NW, normal weight; OB, obese; OW, overweight.

significant contribution to explaining the variance in RIPC to mPFC, and the full model was significant, with systolic BP explaining 1.1% of the variance (Table 2B).

The Kruskal–Wallis *H* test revealed significant BMI group differences, which can be seen in Table 3 and Figure 1. After the pairwise comparison with Bonferroni correction, the overweight group and the obese group significantly differed in the effective connectivity from PCC to mPFC, from PCC to RIPC, and within RIPC, with the overweight group having the highest mean rank value. The normal weight group and the overweight group significantly differed on effective connectivity from LIPC to PCC, from LIPC to mPFC, from LIPC to RIPC, from AI to mPFC, and within RIPC.

The normal weight group had the highest mean rank value for all the connections except for from AI to mPFC, where the overweight group had the highest mean rank value. The normal weight and the obese group significantly differed in effective connectivity from PCC to dorsolateral prefrontal cortex (DLPFC) and from mPFC to RIPC. For PCC to DLPFC, the normal weight group had the highest mean rank value, indicating stronger effective connectivity, whereas the obese group had a higher mean rank value from mPFC to RIPC. As can be seen from Table 3, the effect sizes are low for all the significant different group differences (Cohen, 1988). See Supplementary Table S4 for the non-significant between-group results.

csd parameters

Diastolic BP made a significant contribution toward explaining the variance in the α-value, explaining 1.1% of the variance (Table 2C). The Kruskal–Wallis *H* test revealed no significant group differences on the csd parameters α-value or β-value between the BMI groups; α-value (normal weight $n=262$, overweight $n=202$, obese $n=117$), χ^2 ($df=2$, $n=581$) $=0.439$, $p=0.803$, and β-value (normal weight $n=262$, overweight $n=202$, obese $n=117$), χ^2 ($df=2$, $n=581$) $=2.644$, $p=0.267$.

Free energy

For the free energy parameter, the full regression model explained significantly more variance than gender alone. However, gender made the only significantly unique contribution to the full model. The full model explains around 7.9% of the variance in Free Energy, and BP, HCT, BMI, and HbA1c accounted for 5.0% of the explained variance (Table 2D).

Discussion

Several of our hypothesis, regarding variability in hemodynamic and effective connectivity parameters, were supported. The results of the regression analyses imply that between-subject variance in the hemodynamic parameters of rs-fMRI is predicted by diastolic BP and BMI (in support of H_1). Further, the variance in the effective connectivity within and between rs-networks is predicted by diastolic and systolic BP, HCT, BMI, and HbA1c (in support of H_5, H_6). The between-group comparison for BMI gives insight into hemodynamic and effective connectivity differences between BMI groups (in support of H_2 and H_6).

However, the effect sizes were quite small, as can be seen from the regression analysis with Free Energy, including the independent variable increases the explained model evidence, collectively explaining around 5% of the variance.

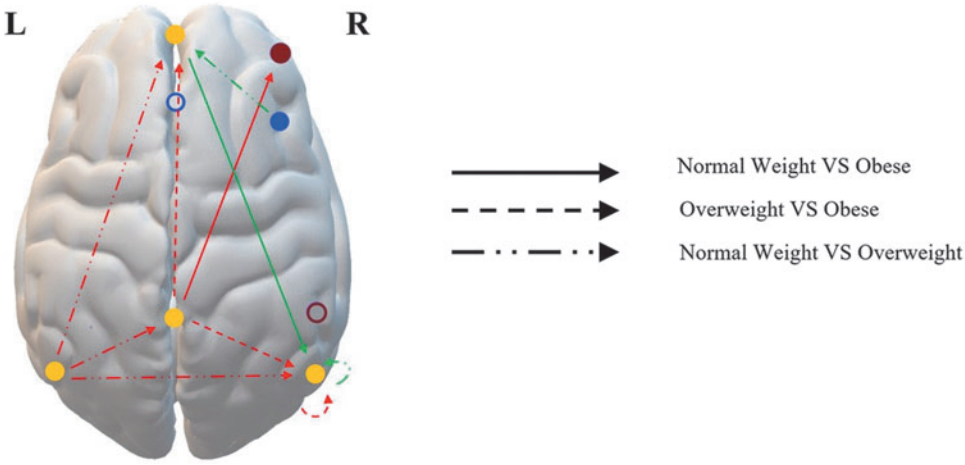

FIG. 1. Illustration of the significant group differences of the Kruskal–Wallis *H* test for the effective connectivity parameters. Please see Table 1 for the exact MNI coordinates for each region. The arrows indicate which groups are being compared, and the directionality of the connection. Based on the mean rank value of the given groups in the comparison, it was determined whether the connection was strengthened (green arrow) or weakened (red arrow) with increased BMI. The color of the solid circles indicates the networks in which the regions showed sig. group differences, with yellow being the DMN (mPFC, PCC, LIPC, RIPC), dark red being the CEN (DLPFC), and blue being the SN (AI). The white circles with a colored border are the regions that did not exhibit significant group differences: PPC (dark red circle, as it is a part of the CEN) and ACC (blue circle, as it is a part of the SN). As can be seen from the figure, all of the affected connections are within the DMN, or between the DMN and the CEN or the SN. Please see Table 3 for the full analysis. ACC, anterior cingulate cortex; AI, anterior insula; CEN, central executive network; DLPFC, dorsolateral prefrontal cortex; DMN, default mode network; LIPC/RIPC, left/right inferior parietal cortex; MNI, Montreal Neurological Institute; mPFC, medial prefrontal cortex; PCC, posterior cingulate cortex; PPC, posterior parietal cortex; SN, salience network.

Hemodynamic parameters: effects of BP and BMI

When including BP in the full regression models, it was found that an increase in diastolic BP has an impact on the shape and amplitude of the BOLD-signal, with a globally increased amplitude of the BOLD-signal, as reflected by the global parameter epsilon and the csd-parameter α, and a local shortening in the regions of mPFC and AI, as indicated by an inverse relationship with the local parameter transit time. The shortened transit times confirm our hypothesis for mPFC and AI, and the hemodynamic signal appears to be altered in all the ROI.

The results indicate that diastolic BP affects the rate at which oHb is being utilized in the capillaries and dHb is transported to the veins, essentially weakening the response from the venous compartments in terms of the Balloon model proposed by Buxton and colleagues (1998). One explanation of this tendency might be related to stiffer venules and veins, which could increase diastolic BP and prevent the Balloon effect (Buxton, 2012; Buxton et al., 1998).

The explanation of the observed variance is, however, probably multifaceted, as the dynamics of the BOLD-signal is complex and generally poorly understood (Arthurs and Boniface, 2002; Ekstrom, 2010; Handwerker et al., 2012; Logothetis and Wandell, 2004). For example, we observed a strong trend for diastolic BP and PPC transit time in the opposite direction of the results for diastolic BP and AI/mPFC.

Increased BMI was found to prolong the BOLD-signal in mPFC whereas the shape/amplitude remained the same, in our regression model. However, the BOLD-signal was shortened in PCC with high BMI in the group comparison analysis (overweight group vs. obese group). A similar trend was found for PCC in the regression model, though only close to significant. Higher BMI is associated with decreased CBV, which is believed to alter the Balloon effect in terms of making the BOLD-signal shorter (Buxton et al., 1998; Lemmens et al., 2006).

As the results from the regression analysis and the group-comparison differ somewhat, in terms of the results' direction, it might be the case that the hemodynamic responses in different brain regions are affected differently by increased BMI.

The effect that BMI and BP have on transit time is not evident in all the regions within the examined rs-networks, but they are limited to mPFC and AI for diastolic BP, and mPFC and PCC for BMI. The mPFC and AI are situated close to two of the big arteries of the brain, namely arteria cerebri anterior and media, which might be one explanation of why these regions appear to be sensitive to differences in hemodynamics. These results are highly intriguing as mPFC and AI are the main hubs of the DMN and the SN, respectively, and, interestingly, as the BOLD signal of mPFC is affected by both diastolic BP and BMI.

Hence, the variability in diastolic BP and BMI might have affected the results of previously conducted functional connectivity studies on the DMN and the SN, while actually being attributable to hemodynamic variability (Rangaprakash et al., 2018).

The amplitude of the low-frequency fluctuations of the rs-fMRI BOLD-signal and the amplitude of the frequency of cardiovascular fluctuations are within the same range: below 0.10 Hz for the BOLD-signal and around 0.08 Hz for the cardiovascular fluctuations (Zhu et al., 2015). The results of the current study are in line with previous results finding the BOLD-signal to be highly coupled with cardiovascular fluctuations and CBF globally, and with regions within the DMN showing the strongest significant coupling (Kobuch et al., 2019; Tak et al., 2014; Whittaker et al., 2019).

Although the amount of explained variance by diastolic BP and BMI alone is fairly low, when considering all of the endogenous and exogenous factors that have been found to affect the connectivity of rs-networks and the BOLD-signal, these components might be contributing factors to the overall low replicability and high variability in rs-fMRI studies.

Effective connectivity

For BP, there was a positive relationship between the diastolic BP and the ''self-inhibitory connection of'' mPFC, which indicates that mPFC is more inhibited with increased diastolic BP. Further, the systolic BP displayed a negative relationship with connections within the DMN, and a positive relationship for the connectivity from the SN to the DMN. The relationships between BP and some of the connections might be related to previous research, which indicated altered connectivity with hypertension in combination with cognitive impairments (Bu et al., 2018).

In the regression analysis, increased BMI predicted a strengthening in one of the connections within the DMN (mPFC to PCC), which is not in line with our hypothesis. By contrast, the comparison of the different BMI groups did, to a large extent, confirm our hypothesis. In short, the results indicate an internal weakening of the connectivity within the DMN with increased BMI, as well as stronger connectivity from the SN to the DMN. The results also indicate that the normal weight group, compared with the obese group, has stronger connections from the DMN to the CEN.

The only connection within the DMN that was stronger with increased BMI in the group comparison was from mPFC to RIPC, for the obese compared with the normal weight group. It should be noted that, when taking the mean rank of all the groups into consideration, a non-linear relationship appears for some of the effective connectivity parameters. This might be why the results of the group comparison differ somewhat from the regression analysis, as it assumes a linear relationship. It might also be why previous research has indicated a linear relationship between higher BMI and changes in rs-connectivity, as most of the studies compare only two groups. This relationship could be further investigated in future studies.

As suggested in previous studies, the results might be reflecting poorly regulated eating behavior, as the networks involved in balancing sensory-driven and internally guided behavior are affected (Doucet et al., 2017; Sadler et al., 2018). The current study contributes to a deeper understanding of the interactions between these networks, as effective connectivity as opposed to functional connectivity is investigated.

It is, for example, interesting to notice that the strengthened connection between AI and mPFC with increased BMI, namely between the SN and the DMN, is, in fact, in the direction from the SN to the DMN. In addition, connections from LIPC to several regions in the DMN appear to be

weaker with increased BMI, which might indicate that LIPC mediates the weakened connectivity in the other regions of the DMN (PCC, mPFC, and RIPC).

As expected, the internal connectivity of the DMN was weakened by increased HCT. The authors are, however, not confident in determining why this relationship arises. Initially, it could be considered as related to the sex differences observed in rs-networks (Agcaoglu et al., 2015), as there are sex differences in normal HCT scores (Murphy, 2014). However, HCT does not explain significantly more than gender for the connection (LIPC to RIPC). Previous studies have indicated that HCT accounts for a weakening of the internal cohesiveness of all of the rs-networks included in this study (Yang et al., 2015).

As the assumptions of regression were only met for LIPC to RIPC, it was the only conducted analysis with HCT, thus not allowing for testing whether there is a weakening of the internal connectivity of all the included networks. However, one might consider the correlation analysis as indicative of minimal relationship between HCT and the effective connectivity of the rs-networks.

HbA1c exhibited a positive relationship with the effective connectivity from the DMN to the SN, which is not in line with our *a priori* hypothesis, but might, as for BMI, be related to regulatory mechanisms for eating behavior. A weakening of the internal connectivity in the CEN and the SN was, however, not observed. Previous research has indicated altered connectivity in AI and its connections, but in our case the assumptions of regression were not met for many of the analysis that included HbA1c as predictor and connections with AI.

The only one included in a regression model was AI to ACC, and HbA1c did not contribute to explaining the variance in this case. However, the previous results have mostly compared subjects with pre-diabetes or diabetes, as opposed to the normal scores of the current study (Liu et al., 2017; Sadler et al., 2019; Yang et al., 2016).

General discussion

Seen together, the results indicate that all the factors included in this study can affect the underlying connectivity of the resting human brain, and that diastolic BP and BMI specifically can affect the measured BOLD-signal. As the effect sizes and the percent of explained variance are low, these factors are likely to not cause a large degree of variability in the results independently. However, as implied by Free Energy, they might collectively contribute to unreliable results. Further, the current study adds to the growing body of research on rs-fMRI variability, as the results support the notion that variability in the BOLD-signal and connectivity of rs-networks are to be found even within a fairly healthy population.

Taking BP, HCT, BMI, and HbA1c into account when studying rs-networks might thus be advantageous for future studies, to increase the studies' reproducibility. Further, some of the benefits of using DCM are highlighted with the current study. Utilizing the DCM technique enables future studies to assess whether their results arise from neuronal changes, as well as the directionality of these changes, or whether the changes merely represent variation in cerebral hemodynamics.

As the results of this study indicate that the included endogenous factors are associated with changes in the underlying connectivity and hemodynamic variability of rs-networks, it adds to the number of studies that undermine the notion of rs-networks as being stable between subjects in terms of connectivity, as well as being susceptible to hemodynamic variation caused by BP and BMI. Interestingly, the DMN seems to be more affected by individual factors, as it is susceptible to vary with the endogenous factors in both hemodynamic and effective connectivity parameters.

However, one must bear in mind that the current analysis only explored a subset of networks and only the most central nodes of the different networks. Further, all reported effects are between-subject effects and might represent more a trait than a state, whereas within-subject fluctuations might be lower, as demonstrated earlier (Almgren et al., 2018).

However, seen along with results from other studies, the range of potential sources of variability might be one of the reasons why it has been proven a challenge to come to a unified view on the function of the DMN (Agcaoglu et al., 2015; Choe et al., 2015; Curtis et al., 2016; Goldstone et al., 2016; Harrison et al., 2008; Hodkinson et al., 2014; Waites et al., 2005). In addition, the results implicate that the DMN might not inhabit the between-subject stability that it is ascribed when studying clinical deviations (Greicius et al., 2004; Mevel et al., 2011).

Limitations of the current study

Alternative to the current approach might be the use of parametric empirical Bayes (PEB) (Zeidman et al., 2019b), which could not be implemented here for technical reasons. There are some advantages of using PEB with csd-DCM data as compared with other GLMs, and it can therefore be considered a limitation of this study that a more traditional GLM was utilized for the analyses of between-subject effects on the DCM parameters.

Specifically, many of the analyses were not performed with HCT and HbA1c as independent variables, as the assumptions of the regression analysis prevented it. Even for the significant correlations, which ''allowed'' the variables to be entered into the regression analysis, the relationships between the variables were quite low (around 0.10). Using PEB instead would allow for all the scores on all the independent variables to be analyzed with the DCM parameters, to examine their effect. Running several hierarchical regression models also posed a challenge in terms of controlling for multiple testing, which could have been avoided if using PEB.

Further, the current article focuses on variations that originate from between-subject differences. It would be interesting to explore, more explicitly, which of the identified effects are presented also on the within-subject level. However, a longitudinal study demonstrated rather stable within-subject DCM estimations (Almgren et al., 2018), even though the authors did not take into account the possible causes of individual fluctuations.

Also, an extension to larger network models might give new and more differentiated insights, like a recent large-scale DCM approach where they have explored the same networks as the current report, but with more nodes per network (Bajaj and Killgore, 2021). In the current study, only two

regions were included per network for the CEN and the SN. Although these regions are considered central nodes of the given networks, we acknowledge that several other regions could have been included in our analysis.

For the DMN, four regions were chosen, which might be more representative of the network as a whole, as compared with the CEN and the SN. Therefore, we recommend the reader to place more emphasis on the results from the DMN and its connections, and we highlight that further studies should be conducted to clarify the relationship between the endogenous factors included in this study and the CEN and the SN.

Lastly, the analyses were based on the minimally processed dataset. Future studies need to explore more explicitly to which degree the results reported here propagate through different pre-processing and denoising strategies. So far, mostly simulation studies have explored the effect of various types of (physiological) noise on DCM parameter estimates (Bielczyk et al., 2017, 2019). Besides, also residual subject motion has been shown, despite various correction procedures, to affect the estimates of functional connectivity measures (Bolton et al., 2020; Power et al., 2012).

Conclusion

The low cost, short scanning times, and absence of task, which initially made rs-fMRI an intriguing, useful, and popular tool for neuroimaging, come with a price. Evidently, the rs-networks are susceptible to a variety of exogenous and endogenous factors, which makes the results of the studies unreliable and as a consequence, challenging to replicate. This tendency adds to the difficulty of studying and understanding the function of rs-networks such as the DMN and using alterations in rs-networks as a clinical marker of disease.

Along with previous studies and results, the current study is an indicator of the nature of the DMN as showing larger between-subject variability, in which case it is unsurprising that its function seems to ''slip through the fingers'' of the researcher. If rs-networks are to be truly understood, studies should at least take the effect of BP and BMI into account, to ensure more reliable results for the future. By doing so, the researcher would also take a step in the right direction in terms of the ongoing replication crisis.

Authors' Contributions

All people listed as authors have participated sufficiently in the work to take public responsibility for the content, including participation in the concept, design, analysis, writing, or revision of the article.

Author Disclosure Statement

No competing financial interests exist.

Funding Information

The study was financed by the Research Council of Norway (Project No. 276044: *When default is not default: Solutions to the replication crisis and beyond*). Data were provided by the Human Connectome Project, WU-Minn Consortium (Principal Investigators: David Van Essen and Kamil Ugurbil; 1U54MH091657) funded by the 16 NIH Institutes and Centers that support the NIH Blueprint for Neuroscience Research; and by the McDonnell Center for Systems Neuroscience at Washington University.

Supplementary Material

Supplementary Table S1
Supplementary Table S2
Supplementary Table S3
Supplementary Table S4
Supplementary Figure S1

References

Agcaoglu O, Miller R, Mayer AR, et al. 2015. Lateralization of resting state networks and relationship to age and gender. Neuroimage 104:310–325.

Allen EA, Erhardt EB, Damaraju E, et al. 2011. A baseline for the multivariate comparison of resting-state networks. Front Syst Neurosci 5:2.

Almgren H, Van de Steen F, Kühn S, et al. 2018. Variability and reliability of effective connectivity within the core default mode network: a multi-site longitudinal spectral DCM study. Neuroimage 183:757–768.

Arthurs OJ, Boniface S. 2002. How well do we understand the neural origins of the FMRI BOLD signal? Trends Neurosci 25:27–31.

Bajaj S, Killgore WD. 2021. Association between emotional intelligence and effective brain connectome: a large-scale spectral DCM study. Neuroimage 229:117750.

Bielczyk NZ, Llera A, Buitelaar JK, et al. 2017. The impact of hemodynamic variability and signal mixing on the identifiability of effective connectivity structures in BOLD FMRI. Brain Behav 7:e00777.

Bielczyk NZ, Llera A, Buitelaar JK, et al. 2019. Increasing robustness of pairwise methods for effective connectivity in magnetic resonance imaging by using fractional moment series of BOLD signal distributions. Netw Neurosci 3:1009–1037.

Biswal B, Zerrin Yetkin F, Haughton VM, et al. 1995. Functional connectivity in the motor cortex of resting human brain using echo-planar MRI. Magn Reson Med 34:537–541.

Bolton TA, Kebets V, Glerean E, et al. 2020. Agito Ergo Sum: correlates of spatio-temporal motion characteristics during FMRI. Neuroimage 209:116433.

Bressler SL, Menon V. 2010. Large-scale brain networks in cognition: emerging methods and principles. Trends Cogn Sci 14:277–290.

Bu L, Huo C, Xu G, et al. 2018. Alteration in brain functional and effective connectivity in subjects with hypertension. Front Physiol 9:669.

Buckner RL, Andrews-Hanna JR, Schacter DL. 2008. The brain's default network: anatomy, function, and relevance to disease. Ann N Y Acad Sci 1124:1–38.

Buxton RB. 2012. Dynamic models of BOLD contrast. Neuroimage 62:953–961.

Buxton RB, Uludağ K, Dubowitz DJ, et al. 2004. Modeling the hemodynamic response to brain activation. Neuroimage 23: S220–S233.

Buxton RB, Wong EC, Frank LR. 1998. Dynamics of blood flow and oxygenation changes during brain activation: the Balloon model. Magn Reson Med 39:855–864.

Carnevale L, Maffei A, Landolfi A, et al. 2020. Brain functional magnetic resonance imaging highlights altered connections and functional networks in patients with hypertension. Hypertension 76:1480–1490.

Chao S-H, Liao Y-T, Chen VC-H, et al. 2018. Correlation between brain circuit segregation and obesity. Behav Brain Res 337:218–227.

Choe AS, Jones CK, Joel SE, et al. 2015. Reproducibility and temporal structure in weekly resting-state FMRI over a period of 3.5 years. PLoS One 10:e0140134.

Cohen JW. 1988. *Statistical Power Analysis for the Behavioral Sciences*, 2nd ed. Hillsdale, NJ: Lawrence Erlbaum Associates.

Craig AD. 2009. How do you feel—now? The anterior insula and human awareness. Nat Rev Neurosci 10:59–70.

Curtis BJ, Williams PG, Jones CR, et al. 2016. Sleep duration and resting FMRI functional connectivity: examination of short sleepers with and without perceived daytime dysfunction. Brain Behav 6:e00576.

Doucet GE, Rasgon N, McEwen BS, et al. 2017. Elevated body mass index is associated with increased integration and reduced cohesion of sensory-driven and internally guided resting-state functional brain networks. Cereb Cortex 28: 988–997.

Ekstrom A. 2010. How and when the FMRI BOLD signal relates to underlying neural activity: the danger in dissociation. Brain Res Rev 62:233–244.

Fox MD, Snyder AZ, Vincent JL, et al. 2005. The human brain is intrinsically organized into dynamic, anticorrelated functional networks. Proc Natl Acad Sci U S A 102:9673–9678.

Friston K. 2009. Causal modelling and brain connectivity in functional magnetic resonance imaging. PLoS Biol 7:e1000033.

Friston KJ, Kahan J, Biswal B, et al. 2014. A DCM for resting state FMRI. Neuroimage 94:396–407.

Friston KJ, Mechelli A, Turner R, et al. 2000. Nonlinear responses in FMRI: the Balloon model, Volterra Kernels, and other hemodynamics. Neuroimage 12:466–477.

Gauthier CJ, Fan AP. 2019. BOLD signal physiology: models and applications. Neuroimage 187:116–127.

Glasser MF, Sotiropoulos SN, Wilson JA, et al. 2013. The minimal preprocessing pipelines for the Human Connectome Project. Neuroimage 80:105–124.

Goldstone A, Mayhew SD, Przezdzik I, et al. 2016. Gender specific re-organization of resting-state networks in older age. Front Aging Neurosci 8:285.

González-Alonso J, Mortensen SP, Dawson EA, et al. 2006. Erythrocytes and the regulation of human skeletal muscle blood flow and oxygen delivery: role of erythrocyte count and oxygenation state of haemoglobin. J Physiol 572:295–305.

Greicius MD, Krasnow B, Reiss AL, et al. 2003. Functional connectivity in the resting brain: a network analysis of the default mode hypothesis. Proc Natl Acad Sci U S A 100:253–258.

Greicius MD, Srivastava G, Reiss AL, et al. 2004. Default-mode network activity distinguishes Alzheimer's disease from healthy aging: evidence from functional MRI. Proc Natl Acad Sci U S A 101:4637–4642.

Handwerker DA, Gonzalez-Castillo J, D'esposito M, et al. 2012. The continuing challenge of understanding and modeling hemodynamic variation in FMRI. Neuroimage 62:1017–1023.

Harrison BJ, Pujol J, Ortiz H, et al. 2008. Modulation of brain resting-state networks by sad mood induction. PLoS One 3: e0001794.

Hodkinson DJ, O'daly O, Zunszain PA, et al. 2014. Circadian and homeostatic modulation of functional connectivity and regional cerebral blood flow in humans under normal entrained conditions. J Cereb Blood Flow Metab 34:1493–1499.

Huang S-M, Wu Y-L, Peng S-L, et al. 2016. Inter-strain differences in default mode network: a resting state fmri study on spontaneously hypertensive rat and Wistar Kyoto rat. Sci Rep 6:21697.

Iso H, Kiyama M, Naito Y, et al. 1991. The relation of body fat distribution and body mass with haemoglobin A1c, blood pressure and blood lipids in urban Japanese Men. Int J Epidemiol 20:88–94.

Kobuch S, Macefield VG, Henderson LA. 2019. Resting regional brain activity and connectivity vary with resting blood pressure but not muscle sympathetic nerve activity in normotensive humans: an exploratory study. J Cereb Blood Flow Metab 39:2433–2444.

Koechlin E, Summerfield C. 2007. An information theoretical approach to prefrontal executive function. Trends Cogn Sci 11:229–235.

Lalande S, Hofman P, Baldi J. 2010. Effect of reduced total blood volume on left ventricular volumes and kinetics in type 2 diabetes. Acta Physiol 199:23–30.

Lemmens HJM, Bernstein DP, Brodsky JB. 2006. Estimating blood volume in obese and morbidly obese patients. Obes Surg 16:773–776.

Levin JM, Frederick B deB, Ross MH, et al. 2001. Influence of baseline hematocrit and hemodilution on BOLD FMRI activation. Magn Reson Imaging 19:1055–1062.

Liu L, Li W, Zhang Y, et al. 2017. Weaker functional connectivity strength in patients with type 2 diabetes mellitus. Front Neurosci 11:e00390.

Logothetis NK, Wandell BA. 2004. Interpreting the BOLD signal. Annu Rev Physiol 66:735–769.

Menon V. 2011. Large-scale brain networks and psychopathology: a unifying triple network model. Trends Cogn Sci 15:483–506.

Menon V, Uddin LQ. 2010. Saliency, switching, attention and control: a network model of insula function. Brain Struct Funct 214:655–667.

Mevel K, Chételat G, Eustache F, et al. 2011. The default mode network in healthy aging and Alzheimer's disease. Int J Alzheimers Dis 2011:535816.

Murphy WG. 2014. The sex difference in haemoglobin levels in adults—mechanisms, causes, and consequences. Blood Rev 28:41–47.

Penny WD. 2012. Comparing dynamic causal models using AIC, BIC and free energy. Neuroimage ;59:319–330.

Power JD, Barnes KA, Snyder AZ, et al. 2012. Spurious but systematic correlations in functional connectivity MRI networks arise from subject motion. Neuroimage 59:2142–2154.

Raichle ME, MacLeod AM, Snyder AZ, et al. 2001. A default mode of brain function. Proc Natl Acad Sci U S A 98:676–682.

Raichle ME, Mintun MA. 2006. Brain work and brain imaging. Annu Rev Neurosci 29:449–476.

Rangaprakash D, Wu G, Marinazzo D, et al. 2018. Hemodynamic response function (HRF) variability confounds resting-state FMRI functional connectivity. Magn Reson Med 80:1697–1713.

Razi A, Kahan J, Rees G, et al. 2015. Construct validation of a DCM for resting state FMRI. Neuroimage 106:1–14.

Sadler JR, Shearrer GE, Burger KS. 2018. Body mass variability is represented by distinct functional connectivity patterns. Neuroimage 181:55–63.

Sadler JR, Shearrer GE, Burger KS. 2019. Alterations in ventral attention network connectivity in individuals with prediabetes. Nutr Neurosci 22:140–147.

Singh KD, Fawcett I. 2008. Transient and linearly graded deactivation of the human default-mode network by a visual detection task. Neuroimage 41:100–112.

Specht K. 2019. Current challenges in translational and clinical FMRI and future directions. Front Psychiatry 10:924.
Sridharan D, Levitin DJ, Menon V. 2008. A critical role for the right fronto-insular cortex in switching between central-executive and default-mode networks. Proc Natl Acad Sci U S A 105:12569–12574.
Stephan KE, Weiskopf N, Drysdale PM, et al. 2007. Comparing hemodynamic models with DCM. Neuroimage 38: 387–401.
Tak S, Wang DJ, Polimeni JR, et al. 2014. Dynamic and static contributions of the cerebrovasculature to the resting-state BOLD signal. Neuroimage 84:672–680.
Toro R, Fox PT, Paus T. 2008. Functional coactivation map of the human brain. Cereb Cortex 18:2553–2559.
Uğurbil K, Xu J, Auerbach EJ, et al. 2013. Pushing spatial and temporal resolution for functional and diffusion MRI in the Human Connectome Project. Neuroimage 80:80–104.
Vaisvilaite L, Hushagen V, Grønli J, et al. 2021. Time-of-day effects in resting-state functional magnetic resonance imaging: changes in effective connectivity and blood oxygenation level dependent signal. Brain Connect. [Epub ahead of print]; DOI: 10.1089/brain.2021.0129.
Van Essen DC, Smith SM, Barch DM, et al. 2013. The WU-Minn Human Connectome project: an overview. Neuroimage 80:62–79.
Van Essen DC, Ugurbil K, Auerbach E, et al. 2012. The Human Connectome Project: a data acquisition perspective. Neuroimage 62:2222–2231.
Waites AB, Stanislavsky A, Abbott DF, et al. 2005. Effect of prior cognitive state on resting state networks measured with functional connectivity. Hum Brain Mapp 24:59–68.
Whittaker JR, Driver ID, Venzi M, et al. 2019. Cerebral autoregulation evidenced by synchronized low frequency oscillations in blood pressure and resting-state FMRI. Front Neurosci 13:433.
Xu F, Li W, Liu P, et al. 2018. Accounting for the role of hematocrit in between-subject variations of MRI-derived baseline cerebral hemodynamic parameters and functional BOLD responses. Hum Brain Mapp 39:344–353.
Yang SQ, Xu ZP, Zhan YF, et al. 2016. Altered intranetwork and internetwork functional connectivity in type 2 diabetes mellitus with and without cognitive impairment. Sci Rep 6:32980.
Yang Z, Craddock RC, Milham MP. 2015. Impact of hematocrit on measurements of the intrinsic brain. Front Neurosci 8:452.
Zeidman P, Jafarian A, Corbin N, et al. 2019a. A tutorial on group effective connectivity analysis, part 1: first level analysis with DCM for FMRI. Neuroimage 200:174–190.
Zeidman P, Jafarian A, Seghier ML, et al. 2019b. A guide to group effective connectivity analysis, part 2: second level analysis with PEB. Neuroimage 200:12–25.
Zhao JM, Clingman CS, Närväinen MJ, et al. 2007. Oxygenation and hematocrit dependence of transverse relaxation rates of blood at 3T. Magn Reson Med 58:592–597.
Zhu DC, Tarumi T, Khan MA, et al. 2015. Vascular coupling in resting-state FMRI: evidence from multiple modalities. J Cereb Blood Flow Metab 35:1910–1920.

Address correspondence to:
Guro Stensby Sjuls
Language Acquisition and Language Processing Lab
Department of Language and Literature
Norwegian University of Science and Technology
Trondheim 7491
Norway

E-mail: guro.s.sjuls@ntnu.no